J. Phys. Chem. 1993, 97, 12805-12810

Laser Ablation of NH_4NO_3

Louise Pasternack and Jane K. Rice*

Code 6111, Chemistry Division, Naval Research Laboratory, Washington, D.C. 20375-5320

Received: August 2, 1993; In Final Form: September 22, 1993®

The laser ablation of ammonium nitrate has been studied, with products collected under low-pressure conditions on a cryogenic argon matrix surface. Relative product populations are analyzed using FTIR spectroscopy. Large effects are observed as the laser fluence and wavelengths are changed. Using 1064-nm pulses or low fluences of 532 nm, NH_3 and HNO_3 are most abundant with smaller (or negligible) quantities of NO, NO_2, and N_2O. At 266 nm and higher fluences of 532 nm, the reactions produce larger populations of NO, NO_2, and small amounts of N_2O. Dimers and other aggregates of H_2O, N_2O, and NO are observed in the FTIR spectra and are attributed to migration in or condensation near the matrix. In addition, isotopic substitution of ^{15}N in the NH_4 and NO_3 components of ammonium nitrate results in some scrambling of the NO and N_2O products but not the HNO_3 product, suggesting that multiple collisions leading to secondary reaction products of the nitrogen oxides are occurring.

Introduction

There has been extensive interest in ammonium nitrate (AN) both because it can be used as an oxidizer in explosives and solid propellants and because it is found in atmospheric aerosols.[1] The thermal decomposition of NH_4NO_3 has been studied for many years, due to its importance as an energetic material,[2,3] and both endothermic and exothermic channels have been identified:

$$NH_4NO_3(s) \rightarrow NH_3 + HNO_3 \qquad \Delta H(298) = 185\ \text{kJ/mol} \quad (1)$$

$$NH_4NO_3(s) \rightarrow N_2O + 2H_2O \qquad \Delta H(298) = -36\ \text{kJ/mol} \quad (2)$$

Rosser et al.[2] proposed the following ionic mechanism for formation of N_2O and H_2O:

$$NH_4^+NO_3^- \leftrightarrow NH_3 + HNO_3 \quad (3)$$

$$2HNO_3 \leftrightarrow NO_2^+ + NO_3^- + H_2O \quad (4)$$

$$NH_3 + NO_2^+ \rightarrow N_2O + H_2O \quad (5)$$

More recently, Brower et al.[3] proposed a similar ionic mechanism for temperatures below 290 °C but at higher temperatures they proposed the following mechanism involving free radicals:

$$NH_4NO_3 \leftrightarrow NH_3 + HONO_2 \quad (6)$$

$$HONO_2 \rightarrow HO^\bullet + NO_2 \quad (7)$$

$$HO^\bullet + NH_3 \rightarrow H_2O + NH_2^\bullet \quad (8)$$

$$NH_2^\bullet + NO_2 \rightarrow NH_2NO_2 \quad (9)$$

$$NH_2NO_2 \rightarrow N_2O + H_2O \quad (10)$$

Recently, Rossi et al.[4] have also studied the decomposition of AN. They observed the decomposition under slow temperature rise (5–10 K/min to 500 K) and low-pressure conditions by Fourier transform infrared (FTIR) monitoring of products collected on a KCl window cooled to 85 K and mass spectrometric monitoring of the residual gases. They only observed NH_3 and HNO_3 products under these conditions.

The mechanisms of AN decomposition in the detonation of energetic materials may be more complicated, due to the sudden large increase in temperature and pressure. In order to more closely approach the conditions in the combustion of energetic materials, more rapid thermolysis of NH_4NO_3 has also been studied.[5,6] Russell and Brill[5] studied the thermolysis under conditions where the sample temperature was ramp-heated at 130 K/s up to 925 K at pressures from 1 to 1000 psi. The reaction becomes exothermic only at high pressures (>500 psi), with N_2O and H_2O as the major products. More recently, Brill et al.[6] studied NH_4NO_3 thermolysis using a temperature-jump method where the rate of heating was 2000 K/s to approximately 675 K. Decomposition products, observed with an FTIR spectrometer, included HNO_3, NH_3, N_2O, NO_2, NO, and H_2O. They measured the rate of production of these species and proposed a reaction scheme to account for these products. Under their conditions (1–33 atm), secondary reactions and heterogeneous chemistry from AN aerosols occur, making it difficult to unambiguously determine the reaction mechanism.

A study of AN decomposition was undertaken to examine decomposition products formed at early times for a typical energetic material. When laser ablation is used as a rapid temperature-jump source and the products are trapped in an argon matrix, data on early decomposition products formed under high-temperature and low-pressure conditions are produced. We sought to determine whether the results from laser ablation were similar to the results from thermal heating and whether some of the primary reactions could be identified either from product populations or from observation of radicals or ions. The effects of varying the energy and the wavelength of the laser (a Nd:YAG laser operated at 1064, 532, and 266 nm) were also measured. Studies of isotopically substituted $^{15}NH_4NO_3$, $NH_4{}^{15}NO_3$, and $^{15}NH_4{}^{15}NO_3$ were initiated to elucidate the decomposition mechanisms of the laser ablation. Additionally, the visible spectroscopy of the plume created by the laser ablation was observed using an optical multichannel analyzer (OMA) in order to identify any excited states that would not be present in thermal heating.

Experimental Section

The NH_4NO_3 is ground to a fine powder and dried at 340 K under vacuum for 4–8 h. The powder (between 0.5 and 1 g) is transferred to a 0.5 in. diameter pellet press under dry nitrogen and pressed to 10 000–15 000 psi. The pellet is then glued to the shaft of a motor which is operated at 2 rpm. The pellet and shaft are mounted inside a vacuum chamber near a cryogenically cooled IR window.

® Abstract published in *Advance ACS Abstracts*, November 1, 1993.

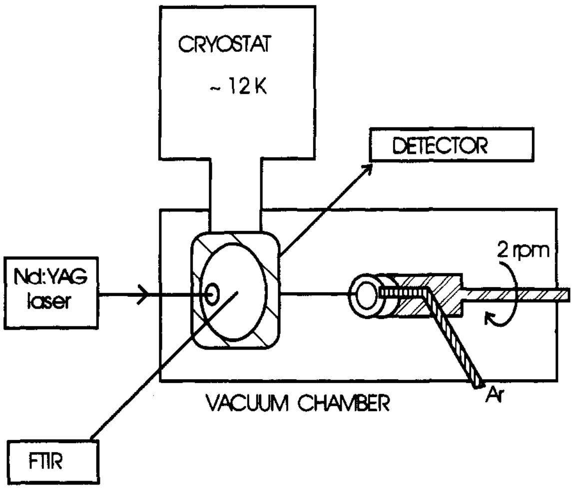

Figure 1. Schematic of the apparatus. A 25-cm lens between the laser and the vacuum chamber is not shown. The pellet position is typically ~2.0 cm from the matrix surface.

The laser ablation/matrix isolation apparatus consists of a closed-cycle helium refrigerator (Air Products, Model DE-202) mounted inside a vacuum chamber, a pulsed (10 Hz) Nd:YAG laser (Quanta Ray, Model DCR-1A) to produce ablation on the rotating samples, an FTIR spectrometer (Mattson, Cygnus 100) to detect species deposited on the matrix, and an OMA (EG&G Model 1460) to characterize the emission from the laser ablation process. A schematic of the apparatus is shown in Figure 1. This is similar to the apparatus described by Burkholder and Andrews.[7] An IR transparent window (1 in. diameter, typically KBr or NaCl) is held in a copper clamp in thermal contact with the refrigerator. A $^1/_8$ in. diameter hole is bored through the window near the edge for transmission of the laser. A cold shield surrounds the window and refrigerator, which maintains the temperature at the window at 10–15 K. The temperature is measured with a gold/chromel thermocouple. For selected spectra, the matrix was annealed by warming the window to 30 ± 5 K for 30–45 min and then cooling again to 10–15 K. No differences in the positions of the spectral features due to annealing were observed, although small losses were observed in signal intensity.

Typical laser energies are ~35–65 mJ for 1064 nm, 20–30 mJ for 532 nm, and 6–12 mJ for 266 nm. During laser ablation, the laser beam impinges on the pellet, which is located about 2.0 cm from the cold window. The laser beam diameters are determined by measuring the spot size burned onto photographic paper mounted at the pellet position. Typical values for the beam diameters are 1.5–2.0 mm for 1064 nm, 0.8–1.2 mm for 532 nm, and 0.3–0.8 mm for 266 nm. The background pressure of the vacuum chamber without matrix deposition is $\sim 1 \times 10^{-7}$ Torr. Argon flow during the matrix deposition yields a pressure of $\sim 1 \times 10^{-5}$ Torr. Argon is flowed at 0.5 sccm through a gas inlet adjacent to the pellet. The argon and ablated material from the pellet are collected on the cold window. The IR absorption of the ablated material is then measured using Fourier transform infrared absorption after 0.5–2 h of deposition using a laser pulse rate of 10 Hz. Spectra are typically recorded at 1-cm^{-1} resolution.

The laser ablation process produces a visible plume. This signal is collected through the slits of a 1/4-m monochromator and measured using an OMA. For 266-, 532-, and 1064-nm ablation, a 300 groove/mm grating is used, resulting in a resolution of ~3 nm. For 266-nm ablation, a 1200 groove/mm grating is also used, resulting in a resolution of ~0.6 nm.

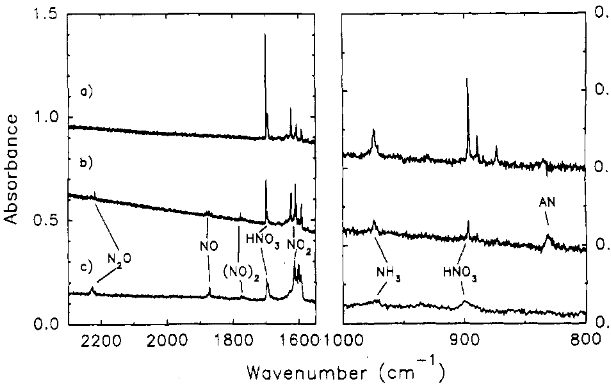

Figure 2. FTIR absorption spectra of laser ablation products, captured on an Ar matrix, for ablation at (a) 1064 nm with 1.6 J/cm^2 fluence, (b) 532 nm with 2.9 J/cm^2 fluence, and (c) 266 nm with 6.5 J/cm^2 fluence.

TABLE I: Frequency and Band Strengths

molecule	vibrational band	Ar matrix frequency (cm^{-1})	band strength (cm^{-2} atm^{-1} at 300 K)
NH_3	ν_2	974[a]	516.8 ± 8.6[b]
HNO_3	ν_1	3519, 3522[c]	
	ν_2	1696, 1699[c]	1393 ± 91[d]
	ν_3	1319, 1321[c]	1259 ± 74[d]
	ν_6	890, 897[c]	630 ± 32[d]
	ν_8	764[c]	
NO_2	ν_3	1612[e]	1400 ± 57[f]
$^{15}NO_2$	ν_3	1578[e]	
NO		1873[e]	112 ± 7[g]
^{15}NO		1841[e]	
c-$(NO)^2$	ν_1	1866[h]	
	ν_5	1778[e]	
c-$(^{14}NO^{15}NO)$	ν_5	1760[e]	
c-$(^{15}NO)_2$	ν_1	1832[h]	
	ν_5	1730[h]	
$^{14}N_2O$	ν_1	1282.9[i]	222 ± 12[j]
	ν_3	2218.6[i]	1402 ± 75[j]
$^{15}N_2O$	ν_3	2149.8[i]	
$^{14}N^{15}NO$	ν_3	2172.6[i]	
$^{15}N^{14}NO$	ν_3	2196.4[i]	

[a] Reference 8. [b] Reference 10. [c] Reference 15. [d] Reference 31. [e] Reference 16. [f] Reference 32. [g] Reference 33. [h] Reference 34. [i] Reference 19. [j] Reference 35.

The NH_4NO_3 samples (Aldrich, 99.999% purity) are used without further purification. Isotopic ammonium nitrates, $^{15}NH_4NO_3$ (98% purity), $NH_4{}^{15}NO_3$ (98% purity), and $^{15}NH_4{}^{15}NO_3$ (98% purity), were obtained from Aldrich and used without further purification. Argon (99.997%) from Air Products was used for the 266-nm, 6.5 J/cm^2 fluence data and argon (99.999% purity) from MG Industries was used for all other data.

Results

1064-nm Laser Ablation. With the ablation laser operating at 1064 nm with a fluence of 1.6 J/cm^2, the major products are found to be NH_3 and HNO_3, as shown in Figure 2. A small amount of the parent molecule is also observed. The vibrational band frequencies used in the spectral identification are listed in Table I. NH_3 is identified from the ν_2 band at 974 cm^{-1}.[8] The other fundamental bands of NH_3 are not observed, but they are expected to be at least 5 times weaker than the ν_2 band.[9,10] NH_3 aggregates with H_2O are also observed at 1035, 3435, and 3702 cm^{-1}.[11-13] HNO_3 is identified from lines near 3505, 1695, 1318, 893, and 764 cm^{-1}.[14,15] Broader bands adjacent to these frequencies were also observed which correspond to a nitric acid dimer and the complex with water.[14] The formation of aggregates will be discussed later. AN, either ablated directly from the pellet or recombined in the plume, is identified primarily from the $NO_3{}^-$ line at 832 cm^{-1} and the broad feature near 1400 cm^{-1}. FTIR spectra of samples containing known percentages of NH_4NO_3 mixed with NaCl were used for spectral identification. Laser ablation at 1064 nm is efficient at removing large quantities of AN due to the wavelength dependence of the laser penetration depth which is proportional to λ^2.

At slightly higher fluences (2.3 J/cm^2) of the Nd:YAG fundamental band, more parent material is ablated. With the

TABLE II: Relative Nitrogen-Containing Product Populations (Percent) from FTIR Spectra at Various Laser Ablation Wavelengths and Fluences

	1064 nm			532 nm		266 nm		
	1.6 J/cm²	2.3 J/cm²	4 J/cm²	2.9 J/cm²	5.8 J/cm²	6.5 J/cm²	11 J/cm²	35 J/cm² [a]
NH_3	31 ± 5	21 ± 7	11 ± 3	7 ± 3	<0.3 ± 0.3	6 ± 2	<3 ± 3	3 ± 1
HNO_3	43 ± 3	25 ± 2	43 ± 5	11 ± 1	0.4 ± 0.3	12 ± 1	11 ± 1	4.7 ± 0.3
NO	<23 ± 23[b]	<46 ± 31[b]	43 ± 22	67 ± 13	88 ± 6	56 ± 9	65 ± 13	77 ± 15
NO_2	<2 ± 2	4 ± 3	2 ± 2	13 ± 2[c]	10 ± 2[c]	20 ± 3[c]	18 ± 3[c]	11 ± 2[c]
N_2O	<3 ± 2	<4 ± 3	<2 ± 2	1 ± 1	1.4 ± 0.4	4.7 ± 0.3	4.2 ± 0.4	3 ± 1

[a] Isotope used here: $NH_4{}^{15}NO_3$. [b] The integrated area is near the limit of detectability, but the band strength is large, leading to a large uncertainty in the percent population. [c] The uncertainty in the integrated area cannot be directly determined due to overlap with water bands and is assumed to be 15%.

laser operating at this fluence, and focused to a diameter of approximately 1.8 mm, 28 ± 7 mg of AN is removed from the pellet after 65 min of ablation with a repetition rate of 10 Hz. This is determined both by weighing the pellet before and after ablation and by estimating the amount of material removed from the groove size. Under these conditions where more energy is deposited in the AN, the predominant nitrogen-containing products are HNO_3 and NH_3, but a small signal due to NO_2 is also observed. The NO_2 was identified from the band near 1611 cm^{-1}.[16] Although there is large overlap in this region from water and water dimer bands,[17,18] this assignment is confirmed using isotopically substituted $NH_4{}^{15}NO_3$. In this case $^{15}NO_2$ with vibrational frequency $\nu_3 = 1578$ cm^{-1} [16] is produced and appears outside the water region.

At higher laser fluences, ~4 J/cm², the HNO_3 signal is reduced in intensity compared to ablation at a lower fluence with most of the signal appearing as nitric acid dimers and aggregates with water. Signals due to NO and *c*-$(NO)_2$ are present, and trace amounts of NO_2 and N_2O are also observed. NO is identified from the line at 1873 cm^{-1}. In addition to monomeric NO, the dimer *c*-$(NO)_2$ is observed at 1866 and 1778 cm^{-1}. These identifications are also confirmed by laser ablating isotopically substituted AN. There are additional lines and a broad underlying absorption in both these regions, most likely due to further aggregation of NO. The N_2O is identified from the band near 2219 cm^{-1}. Absorption due to dimers of N_2O has been observed on both sides of this peak in argon matrices, and higher multimers of N_2O have been identified at 2224.6–2227.8 cm^{-1}.[19] In addition, at higher ratios of N_2O/Ar, Sodeau and Withnall[19] have also observed a broad absorption from the N_2O line extending to approximately 2240 cm^{-1}, which they identify as most likely due to larger aggregates of N_2O, approaching the solid N_2O absorption at 2238 cm^{-1}. H_2O as a product is also observed. In the lower fluence laser ablation experiments at 1064 nm, small signals of water monomers and possibly dimers are observed, which may in part be due to residual water in the apparatus or from small vacuum leaks in the system. At the higher fluence laser ablation, broad signals in both the 3700- and 1600-cm^{-1} regions are observed which we attribute to larger water aggregates though the signal intensities are still modest. There are two much stronger lines which appear at 1593 and 1601 cm^{-1} which we attribute to nonrotating H_2O.[20] Both bands are much more intense under higher laser ablation conditions, in which the ratio of H_2O/Ar is higher and several other species which may enhance these bands are present. The 1593-cm^{-1} band accounts for about 5% of the total integrated signal (not normalized by band strength) at 1064 nm at all fluences and about 10–20% at 532 and 266 nm at all fluences. A dimer H_2O band has also been identified at 1593 cm^{-1}, however, other dimer lines of equal band strength[21] are much weaker in the spectra suggesting that this is a minor contributor. The 1601-cm^{-1} band appears as <5% at 1064 nm with 1.6 and 2.3 J/cm² fluences and is stronger, 12–20% total integrated signal, under all other wavelength and fluence conditions listed in Table II.

Most features in the spectra have been identified, as described. However, there are two bands that are incompletely identified at 3487 and 1309 cm^{-1}. The band at 3487 cm^{-1} is very weak from the ablation of AN at 1064 nm at low fluence (≤2.3 J/cm²) but considerably stronger at higher laser fluence (4 J/cm²). This wavelength can be identified either in the O–H or N–H stretching regions.[22] It is most likely due to an intermolecular O–H hydrogen bond since it shifts slightly with concentration but does not appear to shift due to 532-nm ablation of $^{15}NH_4{}^{14}NO_3$.

At low laser fluence, the band at 1309 cm^{-1} appears in conjunction with the HNO_3 band at 1323 cm^{-1}. However, at the higher fluence, only the 1309-cm^{-1} band appears and it is considerably broadened. The wavelength shifts to 1285–1290 cm^{-1} due to ablation of $NH_4{}^{15}NO_3$. This unidentified band is most likely due to a molecule with an NO_2 stretching frequency band aggregated to water or parent molecules.

The relative concentrations of the nitrogen-containing product species, listed in Table II, are determined from the relative integrated signal intensities normalized by the IR vibrational band strengths[6] listed in Table I. IR band strengths have not been measured for dimers and larger aggregates of H_2O, N_2O, and NO, which account for many of our observed products. Consequently, several assumptions and approximations are necessary to determine the relative concentrations of the product species. We do not attempt to quantify the H_2O population, however, we believe it is a major product for laser fluences over ~3 J/cm². We do calculate the populations of NO and N_2O in spite of aggregation in these cases. The percent composition is obtained by assuming the dimer and aggregates have the same IR absorption intensities as their monomers. For NO, we include the signal due to the monomer and larger aggregates which absorb in the region from 1850 to 1883 cm^{-1}. For N_2O, we also include absorption due to aggregates in the calculations. For NO_2, the region of IR absorption is at 1611 cm^{-1}, which overlaps the water region of the spectra. We estimate the integrated absorption intensity due to the 1611-cm^{-1} band and check it by comparison to values obtained from laser ablation of isotopically substituted $NH_4{}^{15}NO_3$. The $^{15}NO_2$ spectra is shifted out of the water region, to 1578 cm^{-1}.[16] The uncertainties for the relative product populations listed in Table II are determined from an estimate of the uncertainties in the measurement of the integrated absorption intensity combined with the uncertainties in the band strength measurements.

532-nm Laser Ablation. With 532-nm laser ablation, HNO_3, NH_3, NO_2, NO, N_2O, H_2O aggregates, and parent are observed. Aggregation, as previously described, is also observed. Less material is ablated compared to ablation by 1064 nm, due to the shorter penetration depth of 532 nm and the smaller beam diameters. At higher laser fluences, considerably more NO and NO aggregates are observed relative to the other products. HNO_3 and NH_3 signals are much smaller. In addition, at higher laser fluences the absorptions are broadened, which we attribute to greater aggregation. With the laser operating at 27 mJ, and focused to a diameter of approximately 0.8 mm corresponding to a fluence of 5.8 J/cm², 3 ± 1.5 mg of material is removed from the pellet after 0.5 h of ablation with a repetition rate of 10 Hz, estimated from the volume of the pellet groove.

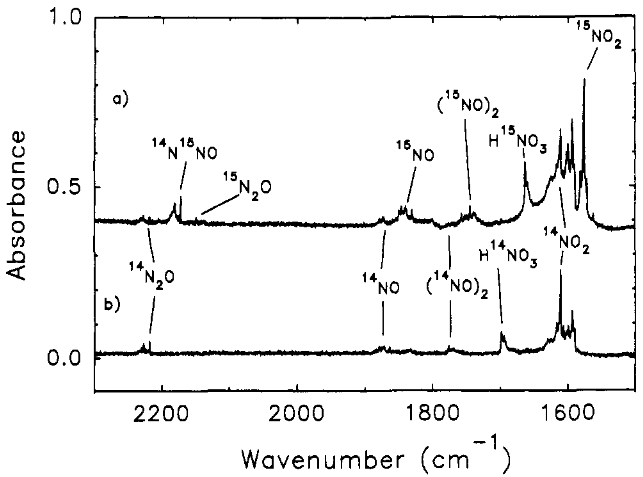

Figure 3. FTIR absorption spectra of the products of 266-nm laser ablation for (a) $^{14}NH_4{}^{15}NO_3$ and (b) $^{14}NH_4{}^{14}NO_3$. The production of mixed isotope species from $^{14}NH_4{}^{15}NO_3$ for the nitrogen oxide species, but not for HNO_3, is noted.

266-nm Laser Ablation. Products of 266-nm ablation include HNO_3, NH_3, NO_2, NO, N_2O, H_2O, and their aggregates. No parent AN is observed. Considerably less material is ablated due to the smaller penetration depth and the smaller laser confocal parameter. The pellet groove is too narrow and too shallow to be measured accurately. We estimate the groove volume from the beam size and the groove depth from the penetration depth for 266-nm ablation compared to 532-nm ablation. Using these estimates, the amount of material removed is calculated to be on the order of 0.3 mg/h using a laser fluence of 11 J/cm^2. For all laser fluences, the product populations vary but the products observed are the same. HNO_3 and NH_3 signals are reduced relative to the water and N_xO_y signals at the higher fluences.

Ablation of Isotopically Substituted Ammonium Nitrate. Studies of isotopically substituted $^{15}NH_4NO_3$, $NH_4{}^{15}NO_3$, and $^{15}NH_4{}^{15}NO_3$ provide additional insight into the mechanism of the ablation, in addition to shifting the NO_2 absorption spectrum away from the water absorption region. The 266-nm ablation of $NH_4{}^{15}NO_3$ results in the production of primarily $^{15}NO_2$, ^{15}NO, c-$(^{15}NO)_2$, and $^{15}N^{15}NO$; however, $^{14}NO_2$, ^{15}NO, c-$(^{15}NO^{14}NO)$, and mixed isotopes of N_2O are also observed, accounting for approximately 25–35% of their respective signals. In the case of N_2O, for example, the integrated absorption signals due to $^{14}N^{14}NO$, $^{14}N^{15}NO$, and $^{15}N^{15}NO$ from the $^{14}NH_4{}^{15}NO_3$ starting material are ~20, 70, and 5%, respectively, with a small amount (<5%) of $^{15}N^{14}NO$ also present. For HNO_3, however, only the $H^{15}NO_3$ isotope is observed. These spectra are shown in Figure 3 and will be discussed later.

Visible Spectroscopy of the Plume from Laser-Ablated NH_4NO_3. The laser ablation process at all three wavelengths produces a small visible plume, indicating that excited atoms or molecules are present. The emission signals from the plumes were dispersed onto an OMA so that they could be compared for the different wavelengths and laser energies used in the ablation. An emission spectrum for 266-nm ablation, with a laser fluence of 35 J/cm^2, is shown in Figure 4. This is a composite of two spectra, taken with the monochromator at different wavelength settings. At all three ablation wavelengths, the spectra consist of a broad continuum with several features superimposed. The continuum spans the region from 350 to 800 nm. The features are identified as due to H, N, and O atomic and ionic emission. The observed spectra are compared to stick spectra for H, N, and O atoms and ions using the transition probabilities[23] for the intensities of the lines as shown in Figure 4. To best fit the data, the H atom transition probabilities were multiplied by a factor of 30 and the O^+ by a factor of 2 relative to the transition probabilities for N^+ and O. No features are attributed to the presence of excited-state diatomic or polyatomic ions or molecules, but these have much smaller transition probabilities than the atoms and atomic ions.

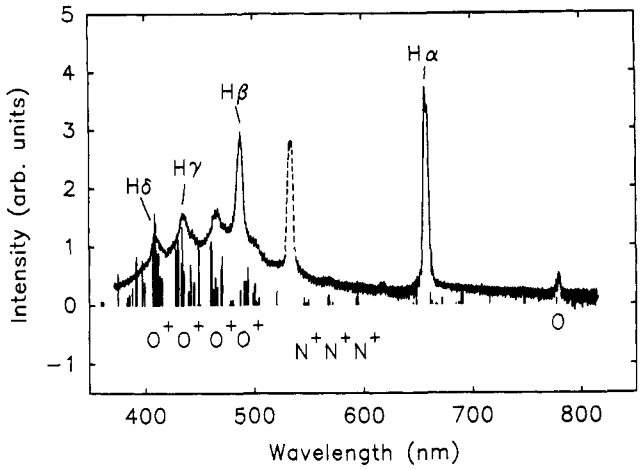

Figure 4. Spectrum of the plume due to 266-nm ablation with ~11. J/cm^2 fluence, measured using an optical multichannel analyzer. The large H atom features are marked. Also shown are the line spectra for O, O^+ and N^+, with intensities calculated from the transition probabilities. The transition probabilities for H have been multiplied by 30 and for O^+ by 2 relative to N^+ and O to best match the observed spectrum. The peak with dashed lines is due to 532-nm scattered laser light.

The effect of two different fluences (6.5 and 35 J/cm^2) on the emission plume is examined using 266-nm excitation. Although the resulting emission spectra are qualitatively similar, the intensity is reduced for the reduced laser fluence, and the peaks, relative to the continuum emission, are somewhat reduced. The peaks due to O and N ions appear to be reduced more than the peaks due to H. A comparison of the emission between 1064- and 266-nm ablation indicates that in the case of 1064-nm ablation (5.8 J/cm^2 fluence), the peaks due to higher energy H atoms are reduced relative to the continuum, but the peaks due to Hα, Hβ, and Hγ are still strong. Signals due to O and N ions appear to be reduced relative to signals due to the H atoms, similar to the emission spectra from the lower fluence 266-nm ablation. The emission spectra due to 532-nm ablation has a large interference due to scattered 532-nm light, making it more difficult to analyze. Peaks due to hydrogen and oxygen are observed, but peaks due to nitrogen fall in the region of the interference.

Discussion

Laser ablation of materials has been observed to produce atoms, radicals, and ions, with many products in electronically excited states.[24] Under our experimental conditions, atomic and ionic species are observed spectroscopically in the plume at high laser fluences, but no radicals or radical ions (such as OH, NH, NH_2, or their ions) are observed either in the plume or in the FTIR spectra of the products from the ablation. The explanation for a lack of radicals or ions observed in the plume may be either that they are not produced or they are masked by the large atom signals. The fact that radicals are not seen in the matrix using FTIR indicates that if they were produced in the plume or multiple collisions have eliminated them before capture. In terms of the stable products, large differences in the product populations occur as the wavelength and fluence of the laser is varied. The fluence is expected to be related to the peak temperature reached in the solid material. The wavelength changes could have a more complicated effect on the product populations, especially if photolysis occurs. The data taken at 1064 nm with low laser fluence is thought to mimic the conditions of pyrolysis most closely, since the photon energy is lowest and a single photon event cannot break chemical bonds. In contrast, at 266 nm, photodissociation of AN is possible. Zawidzki et al.[25] studied the decomposition of AN due to illumination with 254–435-nm light, which resulted in the formation of H_2O, N_2O, N_2, and O_2.

A. Product Populations and Matrix Trapping. *Product Populations and Reaction Mechanisms.* Using 1064-nm pulses, the predominant nitrogen-containing products are HNO_3 and NH_3, especially at lower laser fluences. This is consistent with the observations of Rossi et al.[4] using a slower, thermal heating method. They only observed NH_3 and HNO_3 under their conditions. Using both more rapid heating methods[5] and a T-jump technique,[6] Brill and co-workers also observed NH_3 and HNO_3 as the products evolved at the earliest times and lowest temperatures in their experiments, with AN aerosol and then NO_2, N_2O, NO, and H_2O formed slightly later, at higher temperatures.

Our simplest data at 1.6 J/cm^2 using an ablation wavelength of 1064 nm is similar to the earliest time results of Brill et al.[16] At higher fluences or using 532- or 266-nm ablation, we see the nitrogen oxide species which they observe at later times. However, we observe significantly less N_2O relative to NO or NO_2 and more NO relative to NO_2 than Brill et al.[6] observe at any time. For example, our ratios of N_2O/NO and NO_2/NO at 1064 nm and 4 J/cm^2, are $<0.05/1$ in both cases. Brill et al.[6] report $>3/1$ for N_2O/NO at 656 K in the 5–12 s following rapid heating at 1 atm and from $>1/1$ before 7 s to $\sim 0.5/1$ from 7–12 s for NO_2/NO. A simple picture of our data representing short-time products and theirs representing long-time products probably cannot explain these differences. They may be due to differences in pressure between the two experiments or due to the difference in the temperature distribution and peak temperature from laser ablation compared to the rapid heating method.

Under all wavelength and fluence conditions in our experiments, more HNO_3 is observed than NH_3. Brill et al.[6] also observe this and account for the imbalance by assuming that AN also decomposes to $HNO_3 + N_2 + H_2O$ either directly or by secondary reactions of NH_3 and HNO_3. This consumes more NH_3 than HNO_3. However, the absence of $H^{14}NO_3$ from $NH_4{}^{15}NO_3$ ablation, despite the presence of ^{14}NO, $^{14}NO_2$, and mixed isotopes of N_2O, suggests that reactions of these species do not play a major role in the production of nitric acid under our conditions. We also have evidence that hydrogen atoms are being produced in the ablation process which could account for less NH_3 than HNO_3. Although Rossi et al.[4] observe a slightly larger amount of NH_3 and HNO_3 in their experiments, they attribute it to decomposition of HNO_3 on their trapping surface.

An ionic mechanism[2,3] for reaction 2 has been proposed for lower temperatures (reactions 3–5) and a radical mechanism[3] for higher temperatures (reactions 6–10). We do not identify any of the ionic or radical intermediates in these mechanisms either in the FTIR spectra or in the emission from the plume of the laser ablation. However, in the plume emission, there are broad, featureless regions which could mask these species. We also did not observe the NH_2NO_2 intermediate in the FTIR spectra based on the assignment of the infrared spectrum reported by Rossi et al.[4] and Nonella et al.[26]

In our experiments, there appears to be a threshold for the nitrogen oxide products. Either higher laser fluence or higher energy photons are effective in producing them. A decrease in the NH_3 and HNO_3 products shown in reaction 1 is observed, with a corresponding increase in NO and its aggregates, NO_2, and to a lesser extent N_2O and its aggregates. This can be explained by the higher temperatures presumably reached in the ablation process resulting in an increase in the amount of material ablated and a concomitant increase in the number of collisions before trapping. When N_2O is formed, it does not appear to be in stoichiometric balance with H_2O, as we might expect from reaction 2 alone. Although it is difficult to be quantitative, there appears to be much more H_2O in the form of aggregates. This reinforces the fact that a complex set of reactions are involved in the AN decomposition and at higher fluences and shorter wavelengths more of these reactions appear to occur. UV photolysis of the AN may also play a role although we have no direct evidence for this. As mentioned previously, Zawidzki et al.[25] have observed photodissociation from the UV irradiation of crystalline AN, with H_2O and N_2O as the major products.

TABLE III: Material Removed and Energy Estimates in the Laser Ablation Process

λ (nm)	material removed (g/h)	material removed (mol/shot)	laser energy (mJ)[c]	energy transferred (kJ/(mol shot))
1064	0.028[a]	9.0×10^{-9}	5	3×10^3
532	0.006[a]	2.0×10^{-9}	22	1×10^4
266	0.0003[b]	1.0×10^{-10}	9	8×10^4

[a] Based on the weight of material removed and by laser beam size measurements. [b] Based on beam size measurements only. [c] The laser fluences for these energy measurements are 2.3, 5.4, and 11. J/cm^2 for 1064, 532 and 266 nm, respectively. These are based on beam diameters of 0.17, 0.08, and 0.03 cm, respectively.

From isotopic substitution, it is apparent that approximately 65–75% of the nitrogen oxide species comes directly from the NO_3 part of the AN. Only the HNO_3 species shows no isotopic scrambling. The remainder of the nitrogen oxide species use at least one nitrogen from the NH_4 part. They may be formed from other reactions of AN, for example, those proposed by Brill et al.[6] to account for their observed stoichiometry. They could be explained by collisions of AN molecules coupled with rearrangement or by secondary reactions of NH_x with NO_x or O_x or parent molecules. Under our experimental conditions, the nitrogen oxide species may also be formed from nitrogen atoms or ions, which we observed in the plume.

Species Not Observed. Laser ablation of materials produces atoms, radicals, and ions, in some cases with products in electronically excited states. However, aside from the atoms and atomic ions observed in the plume, there is no evidence of these species in the data presented here. We found no evidence that the following species are present: OH, NH, NH_2, HNO, HONO, HO_2, $O_2N{-}ON{=}O$, *t*-$(NO)_2$, nor O_2NNO.

Aggregation in the Matrix. Many of the products appear as both monomer and dimer and in some cases larger aggregates, for example, N_2O and NO. Some products may also complex with water as we suspect in the case of HNO_3 and NH_3. Under greater laser fluences, more product appears as dimers or aggregates. The laser ablation method used in these experiments may allow collisions to occur between larger ablated particles of the parent material and product molecules or even atoms, contributing to the production of aggregates. In addition, aggregates form in matrices in more concentrated mixtures of solute in solvent, typically when the dilution ratio is below 1:500.[27-29] Since we use a pulsed laser to ablate the AN, the concentration of product species during the laser pulse is relatively high compared to the argon flow, on the order of 1:50 for the 1064-nm ablation, and aggregation at the matrix surface is expected at the matrix surface.

B. Laser Ablation as a Heating Source. *Energy Considerations of Laser Ablation.* Fluences were estimated by measuring the energy and the spot size of the beam, imaged on photographic paper at the pellet. Unfortunately, we do not have a means of measuring the peak pellet temperature in the experimental apparatus. The lowest fluence measurements which lead to the formation of NH_3 and HNO_3 look similar to the data of Rossi et al.[4] in the temperature range 400–500 K. The measurements presented here in which H_2O is released and nitrogen oxides are produced partially resemble the 600–700 K data on AN collected by Brill et al.,[6] however, to define a temperature, there must be a Boltzmann distribution of excited states, which is not the case in the laser ablation process presented here.

We can estimate an upper limit of the energy transferred to the AN from the laser. The results are given in Table III. This calculation is based on the amount of material removed per laser shot and the laser energy measured outside the vacuum chamber. The amounts of material are taken from weight and volume measurements on the pellets after 1064- and 532-nm ablation, as described earlier. For 266-nm ablation, the volume of material removed is estimated relative to 532- and 1064-nm ablation based on the laser beam diameter and the relative penetration depth for the 266-nm data. The amount of energy transferred per laser shot per mole of AN is most likely too high since the mass of material heated is probably greater than the amount actually ablated. In spite of the overestimation in all cases, the relative differences in the energies transferred give some indication of the different ablation conditions at the three wavelengths used in our experiments. The amount of energy deposited in the AN by the 266-nm ablation is considerably higher than that for 1064- or 532-nm ablation, which explains our observation that more "high-temperature" products such as NO, NO_2, and N_2O are present under these conditions. However, the 266-nm spectrum also has attributes of a "low-temperature" measurement indicated by the presence of HNO_3 and NH_3. This may be an indication of the presence of photochemistry or may simply indicate that there are regions in the smaller plume that do not reach the "high temperature". We can estimate the peak temperatures, T_{peak}, for the three wavelengths using the following equation:

$$T_{\text{peak}} = E_{\text{laser}}/(C_p n) \qquad \text{(I)}$$

where E_{laser} is the laser energy, n is the number of moles, and C_p is the heat capacity. The value used for the heat capacity is 139 J/(deg mol).[30] The T_{peak} values obtained from the equation are 4×10^4, 1×10^5, and 6×10^5 °C, for ablation at 1064 (2.3 J/cm^2), 532 (5.4 J/cm^2) and 266 nm (11. J/cm^2), respectively. This provides only a rough approximation of the "peak temperature" assuming no heat loss mechanisms. This does not address the distribution of temperature present nor give the "average temperature" of the laser-ablated material.

We can gain an independent estimate of the amount of energy transferred in the laser ablation process from the energy required to produce the atoms and ions we observe in the emission spectra. Hydrogen atoms, excited on the Hγ line, have 1.26×10^3 kJ/mol energy. It requires approximately an additional 450 kJ/mol to break the chemical bond for a hydrogen atom, making the total 1.7×10^3 kJ/mol for the lower limit to the energy required for excited hydrogen atoms, which we observe at all three wavelengths for ablation. Approximately 4.8×10^3 kJ/mol is required to produce excited oxygen ions, which we also observe at all three wavelengths, although relatively less is observed due to 1064-nm ablation and due to lower energy 266-nm laser ablation. More than 5×10^3 kJ/mol of energy is required to produce excited nitrogen ions, since three H–N bonds must be broken. These numbers are on the same order of magnitude as the estimates of energy transferred from material ablated.

Heterogeneous Reactions. The laser ablation method used here may allow collisions to occur between larger ablated particles of the parent material and product molecules or even atoms. It is not clear how important such heterogeneous reactions are in the normal detonation of these materials and whether the conditions here, at much lower pressures, are a resonable approximation to the early stages in the decomposition or detonation processes. This would require further study.

Summary

A study of ammonium nitrate is presented in which laser ablation is used as a rapid temperature-jump source, products are collected under low-pressure conditions (1×10^{-5} Torr) on a cryogenic argon matrix surface ($\sim$15 K), and relative product populations are analyzed using FTIR spectroscopy. Large effects are observed as the laser fluence and wavelengths are changed which can be attributed to the differences in the amount of energy transferred to the AN. There appears to be a threshold for formation of nitrogen oxide species. These species are present only with higher energy photons or at higher laser fluences. Many products appear both as monomer and complexed as dimer or with H_2O, presumably due to aggregation at the matrix surface. Although atoms and atomic ions are observed directly in the plume, only stable species are observed on the matrix, not atoms, ions, or radicals such as OH or NH, suggesting the presence of secondary reactions in the plume region and on the way to the matrix. The observation of isotopically scrambled products from the ablation of isotopically substituted AN also supports the presence of secondary reactions or the reaction of atoms from the laser ablation. Further studies are needed to characterize the mechanism of the production of isotopically scrambled species.

The laser ablation technique offers a degree of variability in the amount of energy deposited into the energetic material thus allowing the study of these materials under different "heating" conditions. The amount of energy deposited in the material appears to affect both the final "temperature" of the AN as well as the amount of product ablated and hence the number of secondary collisions.

Acknowledgment. We thank Lester Andrews for his advice on the experimental apparatus. We also thank Jeff Owrutsky for helpful discussions on the vibrational analysis, Zakya Kafafi for helpful discussion on the apparatus, Tom Brill for band strength values, and Tom Russell for reading the manuscript. Funding for this work was provided by the Office of Naval Research.

References and Notes

(1) Petriconi, G. L.; Papee, H. M. *J. Atmos. Sci.* **1970**, *27*, 164.

(2) Rosser, W. A.; Inami, S. H.; Wise, H. *J. Phys. Chem.* **1963**, *67*, 1753.

(3) Brower, K. R.; Oxley, J. C.; Tewari, M. *J. Phys. Chem.* **1989**, *93*, 4029.

(4) Rossi, M. J.; McMillen, D. F.; Golden, D. M. SRI Project 8999, Contract No. N00014-90-C-0115, 1992.

(5) Russell, T. P.; Brill, T. B. *Combust. Flame* **1989**, *76*, 393.

(6) Brill, T. B.; Brush, P. J.; Patil, D. G. *Combust. Flame* **1993**, *92*, 178.

(7) Burkholder, T. R.; Andrews, L. *J. Chem. Phys.* **1991**, *95*, 8697.

(8) Cugley, J. A.; Pullin, A. D. E. *Spectrochim. Acta* **1972**, *29a*, 1665.

(9) Pimentel, G. C.; Bulanin, M. O.; Van Thiel, M. *J. Chem. Phys.* **1962**, *36*, 500.

(10) Kim, K. *J. Quant. Spectrosc. Radiat. Transfer* **1985**, *33*, 611.

(11) Abouaf-Marguin, L.; Jacox, M. E.; Milligan, D. E. *J. Mol. Spectrosc.* **1977**, *67*, 34.

(12) Engdahl, A.; Nelander, B. *J. Chem. Phys.* **1989**, *91*, 6604.

(13) Nelander, B.; Nord, L. *J. Phys. Chem.* **1982**, *86*, 4375.

(14) Ritzhaupt, G.; Devlin, J. P. *J. Phys. Chem.* **1977**, *81*, 521.

(15) Cheng, B.-M.; Lee, J.-W.; Lee, Y.-P. *J. Phys. Chem.* **1991**, *95*, 2814.

(16) Jacox, M. E.; Miligan, D. E. *J. Mol. Spectrosc.* **1973**, *48*, 536.

(17) Fredin, L.; Nelander, B.; Ribbegard, G. *J. Chem. Phys.* **1977**, *66*, 4065.

(18) Bentwood, R. M.; Barnes, A. J.; Orville-Thomas, W. J. *J. Mol. Spectrosc.* **1980**, *84*, 391.

(19) Sodeau, J. R.; Withnall, R. *J. Phys. Chem.* **1985**, *89*, 4484.

(20) (a) Ayers, G. P.; Pullin, A. D. E. *Spectrochim. Acta* **1976**, *32A*, 1629. (b) Ayers, G. P.; Pullin, A. D. E. *Spectrochim. Acta* **1976**, *32A*, 1641.

(21) Chin, S.; Ford, T. A. *THEOCHEM* **1985**, *133*, 193.

(22) Socrates, G. *Infrared Characteristic Group Frequencies*; John Wiley and Sons: New York, 1980; p 5.

(23) Weast, R. C.; Astle, M. J.; Beyer, W. H., Eds. *CRC Handbook of Chemsitry and Physics*, 68th ed.; CRC Press: Boca Raton, FL, 1987; pp E-329–E-353.

(24) Cheung, J.; Horwitz, J. *MRS Bull.* **1992**, *17*, 30.

(25) Zawidzki, T. W.; Petriconi, G. L.; Papee, H. M. *Nature* **1965**, *207*, 262.

(26) Nonella, M.; Muller, R. P.; Huber, J. R. *J. Mol. Spectrosc.* **1984**, *112*, 142.

(27) Meyer, B. *Low Temperature Spectroscopy*; American Elsevier Publishing Company Inc.: New York, 1971; p 208.

(28) Suzer, S.; Andrews, L. *J. Chem. Phys.* **1987**, *87*, 5131.

(29) Tso, T.-L.; Lee, E. K. C. *J. Phys. Chem.* **1985**, *89*, 1612.

(30) Dean, J. A., Ed.; *Lange's Handbook of Chemistry*; McGraw-Hill Book Co.: New York, 1985; Section 9, p6.

(31) Giver, L. P.; Valero, F. P. J.; Goorvitch, D.; Bonomo, F. S. *J. Opt. Soc. Am. B* **1984**, *1*, 715.

(32) Devi, V. M.; Fridovich, B.; Jones, G. D.; Snyder, D. G. S.; Das, P. P.; Flaud, J.-M.; Camy-Pegret, C.; Rao, K. N. *J. Mol. Spectrosc.* **1982**, *93*, 179.

(33) Falcone, P. K.; Hanson, R. K.; Kruger, C. H. *J. Quant. Spectrosc. Radiat. Transfer* **1983**, *29*, 205.

(34) Nour, E. M.; Chen, L.-H.; Strube, M. M.; Laane, J. *J. Phys. Chem.* **1984**, *88*, 756.

(35) Kagann, R. H. *J. Mol. Spectrosc.* **1982**, *95*, 297.